Chapter 7
Effect of Far-Field Structure on Joint Properties

S.B. Cooper, M. Rosatello, A.T. Mathis, K. Johnson, M.R.W. Brake, Matthew S. Allen, A.A. Ferri, D.R. Roettgen, B.R. Pacini, and Randall L. Mayes

Abstract Classical structural analysis techniques have proven time and time again to be remarkably accurate for systems consisting of a single, continuous piece of material. Unfortunately, nearly all real engineering structures are assembled from multiple parts, joined by bolts, rivets, or other fasteners, and these joints introduce nonlinearities and uncertainties into systems' structural stiffness and damping. Nonlinear damping due to jointed connections in particular is critical to limiting the resonant response of a structure, yet it remains poorly understood. This work seeks to understand the degree to which joint properties are dependent on the rest of the structure. The testable hypothesis is that the boundary conditions and the far-field structure itself (i.e. distribution of the stiffness and mass) change the way in which the interface is loaded, thus altering the perceived or deduced nonlinear properties of the mechanical joint. This hypothesis is investigated using experimental impact hammer testing methods in order to understand the extent to which alteration in the boundary conditions and far-field structure change the interface properties as well as the underlying mechanics during loading. Numerical tools are also employed to investigate and complement the experimental results, focusing on two fronts: replicating the experimental results with discrete joint models, and investigating joint loading for different modes using numerical modal analysis.

Keywords Jointed structures • Nonlinear stiffness • Nonlinear damping • Hilbert transform and Impact modal test

S.B. Cooper (✉)
Department of Mechanical Engineering, University of Bristol, Bristol, UK
e-mail: sc14784@bristol.ac.uk

M. Rosatello
Laboratoire Quartz – EA 7393, SUPMECA, Saint-Ouen, France

A.T. Mathis
Department of Mechanical Engineering, University of Akron, 44325, Akron, OH, USA

K. Johnson
University of New Mexico, 87131, Albuquerque, NM, USA

Sandia National Laboratories, 87123, Albuquerque, NM, USA

M.R.W. Brake
Sandia National Laboratories, Albuquerque, NM, USA

William Marsh Rice University, Houston, TX, USA

M.S. Allen • D.R. Roettgen
Department of Engineering Physics, University of Wisconsin, Madison, WI 53706, USA

A.A. Ferri
Department of Mechanical Engineering, Georgia Tech, 30332, Atalanta, GA, USA

B.R. Pacini
Sandia National Laboratories, PO Box 5800, 87185, Albuquerque, NM, USA

R.L. Mayes
Structural Dynamics Department, Sandia National Laboratories, P.O. Box 5800 – MS0557, Albuquerque, NM 87185, USA

M.S. Allen et al. (eds.), *Dynamics of Coupled Structures, Volume 4*, Conference Proceedings of the Society for Experimental Mechanics Series, DOI 10.1007/978-3-319-54930-9_7

7.1 Introduction

Most real-world structures do not consist of a single piece of engineering material; instead, they are built-up structures containing several individual pieces constrained by mechanical connections. Despite their prevalent use, distributed contact connections such as joints, have long been difficult to characterize and model due to their nonlinear, stochastic nature. To compound matters, estimation of damping due to friction in mechanicals joints is often extremely important in high-performance applications such aerospace. As a result, many works have studied mechanical joints using analytical, numerical, and experimental methods in an effort to derive quantitative descriptions for these complex engineering systems.

Perhaps one of the most well-known works in the academic community is that of Segalman [9], where he proposes and derives a physically-based joint model using discrete arrangements of Jenkins elements, with the arrangements sometimes called Iwan elements in this context. His so-called four-parameter Iwan element is oft cited and utilized by the joints research community, as it has demonstrated the ability to qualitatively and quantitatively match certain experimental data. Roettgen et al. [8] demonstrated this for the first few modes of an automotive exhaust structure, and Allen et al. [1] developed a quasi-static approach so these types of models can be extracted more efficiently from computational models. Other reduced-order models are proposed by authors such as Quinn [7], which utilize continuum representations of both the monolithic structure and joint to derive computationally inexpensive models. Relatedly, authors have also explored the presence, or absence, of energy transfer through mode coupling, an important physical phenomenon when discussing joint characterization [4, 8]. Regardless of method or characterization technique, the literature recognizes that energy dissipation versus forcing amplitude in these systems is generally governed by a power-law, with hysteresis playing an important role.

Each of these modeling and characterization approaches has its own set of advantages and limitations; however, these works all, cumulatively focus on describing the joint itself with less regard for the surrounding, or far-field, structure. Comparatively little work has been done to assess the impact that the individual components of the built-up structure have on the nonlinear characteristics of the joint. Put another way, there is opportunity to explore the degree to which a joint's excitation, or activation, is affected by the far-field structure in a built-up system. To address that question, this work utilizes experimental methods, data-processing techniques, and numerical simulations that are current to the literature in order to characterize the nonlinear properties of nominally identical joints in structures with different far-fields.

For the experimental portion of this work, several structures with nominally identical joints and different far-field structures were excited using impact hammer testing, and the responses of those structures were identified and characterized using the aforementioned methods currently available in the literature. The basic structure of interest to this work is the Brake-Reuß Beam (BRB), and to address the effect of the far-field structure, several variations of the structure were also created with the hope of altering the response while the joint setup remained constant. These variations include an elongated BRB (LBRB) as well as a stiffness modified BRB (SBRB); details and diagrams of these structures are given in Sect. 7.2.1. This beam-structure was chosen due to the plethora of data available for comparison and its consistent use by authors in the field [2]. For the nonlinear characterization, the Hilbert transform method outlined in Kerschen's work [5] and using the smoothing process described in Roettgen et al. [8] was employed. These modal results are drastically different among the different beams, but the experimental data alone does not give an understanding as to why these modal results are so different.

To complement the experimental studies for this work, numerical methods were also employed in order to better understand the underlying physics of the system. A finite element model using discrete, physical four-parameter Iwan elements was generated and tuned to match the experimental nonlinear, modal damping and natural frequency versus amplitude that were measured from the nominal structure (the classic Brake-Reuß beam) [1]. These same physical joint parameters were then used in a model for the LBRB and the numerical modal nonlinear characterizations match remarkably well. This result implies that, despite the structural modifications, the underlying representative joint properties remain identical.

7.2 Experimental Investigation

The core of this work is the experimental investigation of three different structures with nominally identical joints. First, the design of those structures is discussed, followed by the linear then nonlinear experimental analyses. The linear experimental analysis was designed to identify the appropriate modal filter for the nonlinear characterization, and further details of the characterization method are discussed. Experimental results are shown for the first several modes of the systems, with an emphasis on the lowest three bending modes.

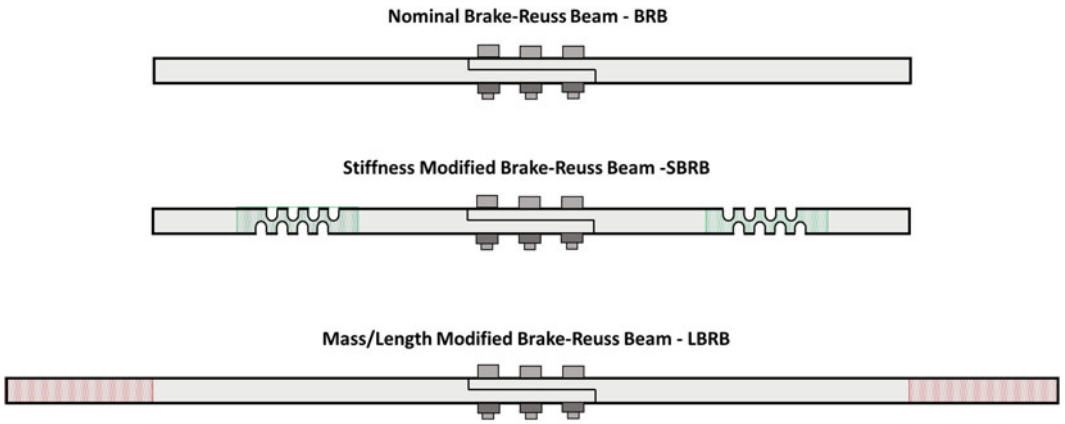

Fig. 7.1 The different beam assemblies

Table 7.1 Dimensions of tested beams

	L × H × W [mm]
BRB – nominal Brake Reus beam	720 × 25.4 × 25.4
SBRB – stiffness modified beam	720 × 25.4 × 25.4
LBRB – mass/length modified beam	1080 × 25.4 × 25.4

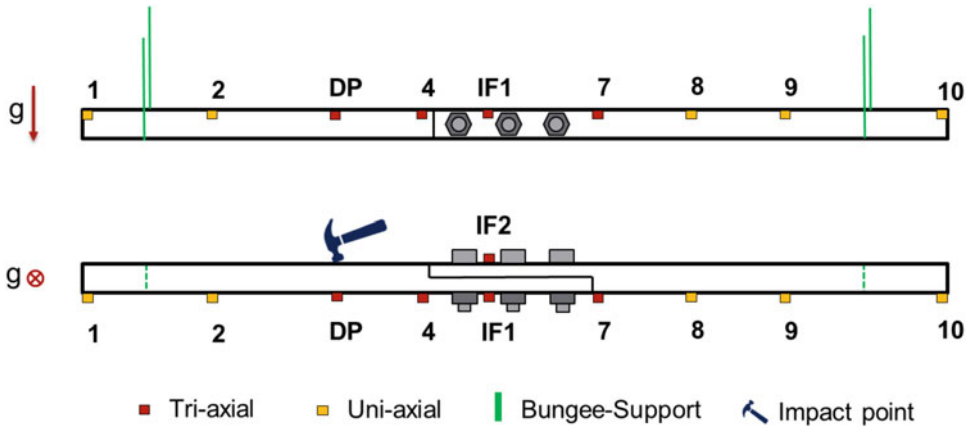

Fig. 7.2 Experimental setup

7.2.1 Experimental Setup

Three different structures were designed for this investigation in order to understand the effect of changing the geometrical properties around a mechanical joint. The first structure is known as the Brake-Reuss beam (BRB) (see [2]); it consists of two identical steel beams bolted together to form a lap-joint connection, assembled using three M8 bolts tightened to a torque of 20 Nm.

The second test structure is similar to the first lap-joint configuration, with the same bolts and torque, however each identical steel beam in this assembly has a spring shaped cut out for stiffness modification. The last test structure also consists of the same lap-joint configuration, but the length of the two parts is larger to provide mass/length modifications. Figure 7.1 shows the three tested beam assemblies configurations and Table 7.1 presents their dimensions. For simplicity, for each beam was assigned an acronym that will be used throughout this paper: BRB for the nominal Brake-Reuss Beam, LBRB for the mass/length modified beam and SBRB for the stiffness modified beam.

Figure 7.2 shows the experimental configuration for the BRB structure. The structure is supported by two bungee cords, and 10 accelerometers were distributed in a symmetrically proportional way on the beam. The chosen source of excitation is the impact hammer: this is commonly used in vibration testing, as it applies a broadband excitation signal to the test structure. The excited band spans within 0–3200 Hz to encompass as many modes as possible. The chosen impact point, or

Table 7.2 Natural frequencies and damping from linear modal analysis

	BRB		LBRB		SBRB	
MODE	f_n [Hz]	ζ (%)	f_n [Hz]	ζ (%)	f_n [Hz]	ζ (%)
1	168.3	0.24	80.5	0.17	92.1	0.12
2	584.3	0.16	291.6	0.05	194.6	0.05
3	1183.8	0.14	521.2	0.07	504.6	0.16
4	1618.3	0.20	857.9	0.19	958.9	0.09
5	1656.3	0.20	1142.9	0.11	1240.2	0.11
6	2825.9	0.15	1339.5	0.05	1623.7	0.16
7	3022.6	0.15	1583.6	0.23	2088.6	0.12

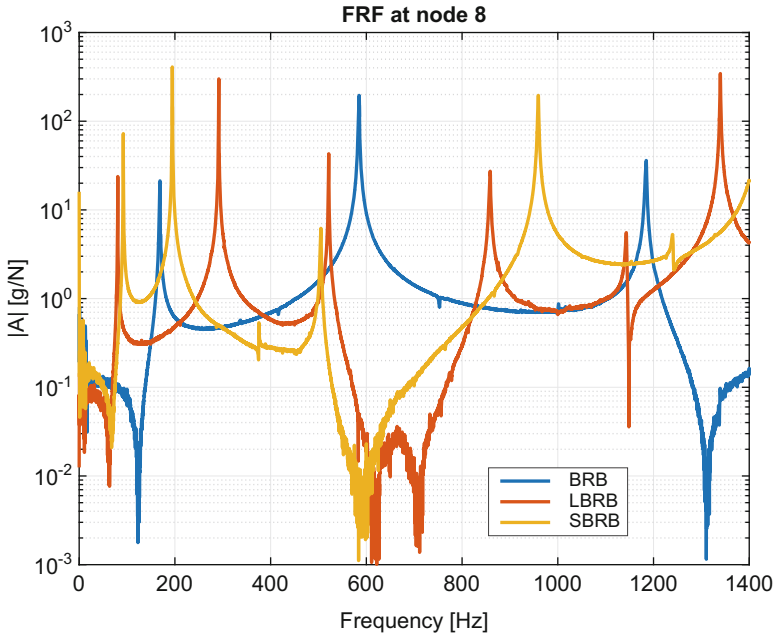

Fig. 7.3 FRF comparison at node 8

driving point (DP), is shown in Fig. 7.2. The SBRB was instrumented in the same way due to the fact that it has similar dimensions to the BRB; however because LBRB is longer than the other two, the accelerometers were attached at positions proportionally consistent with the other two systems. The data acquisition was performed using the Spectral Test module in LMS Test Lab 13.

7.2.2 Linear Experimental Analysis

In order to derive the modal filter used in the nonlinear characterization of these systems, a linear modal test was performed for all three configurations of the beam assemblies. A low level excitation test (F = 50N) was carried out for each beam. The linear natural frequencies and damping ratios were estimated from the frequency response functions (FRFs), using the frequency-domain subspace identification algorithm presented in [6]. Results are shown in Table 7.2. Figure 7.3 shows the FRFs obtained from node 8 of each beam in the range 0–1400 Hz. It is possible to observe that the responses of the three beams are very different between each other as a result of the far-field structure modifications. For example, the first bending mode of the BRB is at 168.3 Hz, for the LBRB is at 80.5 Hz, while for the SBRB is at 92.14 Hz. Furthermore, the steep resonance peaks of the FRFs indicates that the structure is lightly damped across the selected bandwidths. The authors have selected the first three bending modes for each beam assembly to be investigated further in this paper.

The mode shapes for the first three bending modes of interest are obtained from the linear modal analysis for each beam, and they are shown in Fig. 7.4. Comparing these mode shapes, it is clear that the far-field structure modifications have a large impact on the curvature of the linear modes, as expected. For all three modes, the LBRB appears to have a qualitatively similar overall shape to the original BRB. For the first mode, this can be identified more specifically by noting the generally

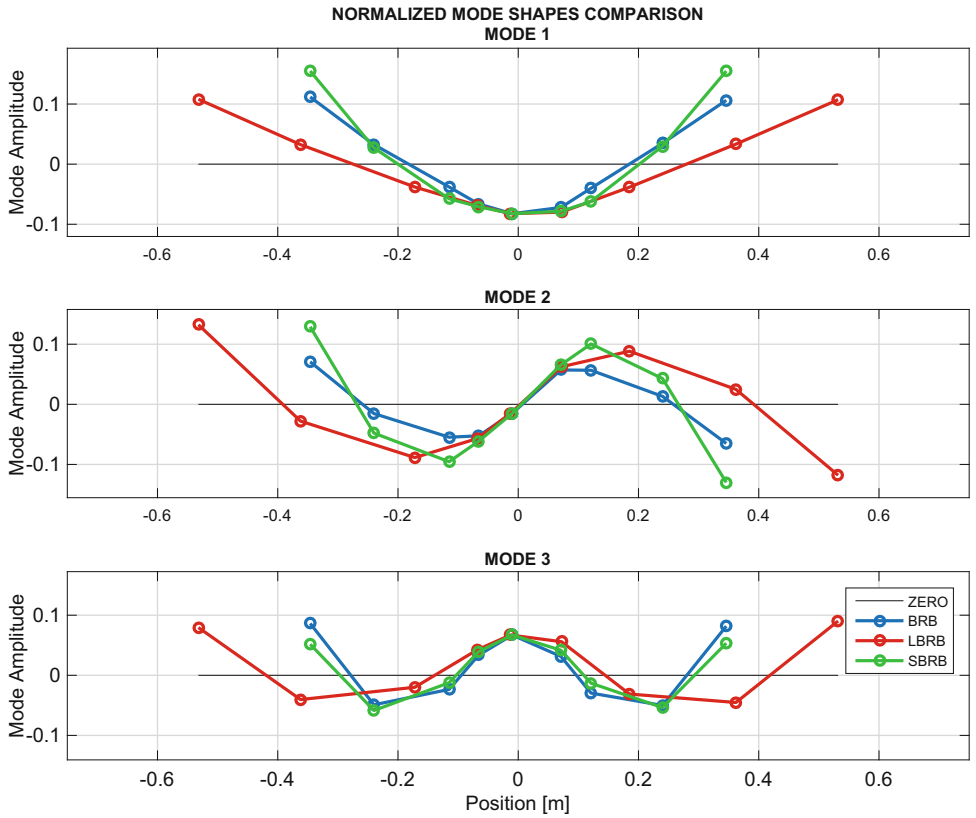

Fig. 7.4 Mode shapes for the three beams

larger radii of curvature in both the BRB and LBRB. By contrast, the SBRB mode shapes exhibit fundamental differences from the other two. Again, in the case of the first mode, the SBRB exhibits lower curvature near the joint area and higher curvature near the ends than the BRB and LBRB.

7.2.3 Nonlinear Experimental Analysis

After the linear modal analysis, the second type of investigation performed was a series of impact tests at increasing force levels in order to elicit nonlinear behavior in the different beams. Each beam was excited at the same impact point DP (see Fig. 7.2), and several impact excitation levels ranging from 50N to 750N were performed. This section details approximate nonlinear characterizations through peak-picking methods in order to illustrate the differences between the linear and nonlinear responses while Sect. 7.2.4 details a more rigorous analysis using the Hilbert Transform method.

7.2.3.1 Impact Test Characterization

Time response signals and frequency response functions (FRFs) were obtained from each test at each forcing level; Fig. 7.5a shows the time response at several excitation forces of the BRB at node 8. As an initial and simplified method to detect nonlinearities in the system, the collected FRFs at increasing impact forces were superposed and compared for each beam: Fig. 7.5b–d show the results of this process at node 8 for the first bending mode and for each beam.

The first observation that can be made is evident in Fig. 7.5a, where an absence of proportionality is noticed between the time responses at low (50N) and high (700N) excitation forces. This indicates the breakdown of superposition principle which serves as a cornerstone for linear theory. Beyond time series inspection, another meaningful method of detecting nonlinear behavior from measured data is the check for homogeneity in the frequency response functions over different excitation levels. In particular, Fig. 7.5b–d show a shift in the natural frequencies and response amplitude as the impact force increases. The characteristics observed from the extracted FRFs show that each beam assembly has a softening behavior within the

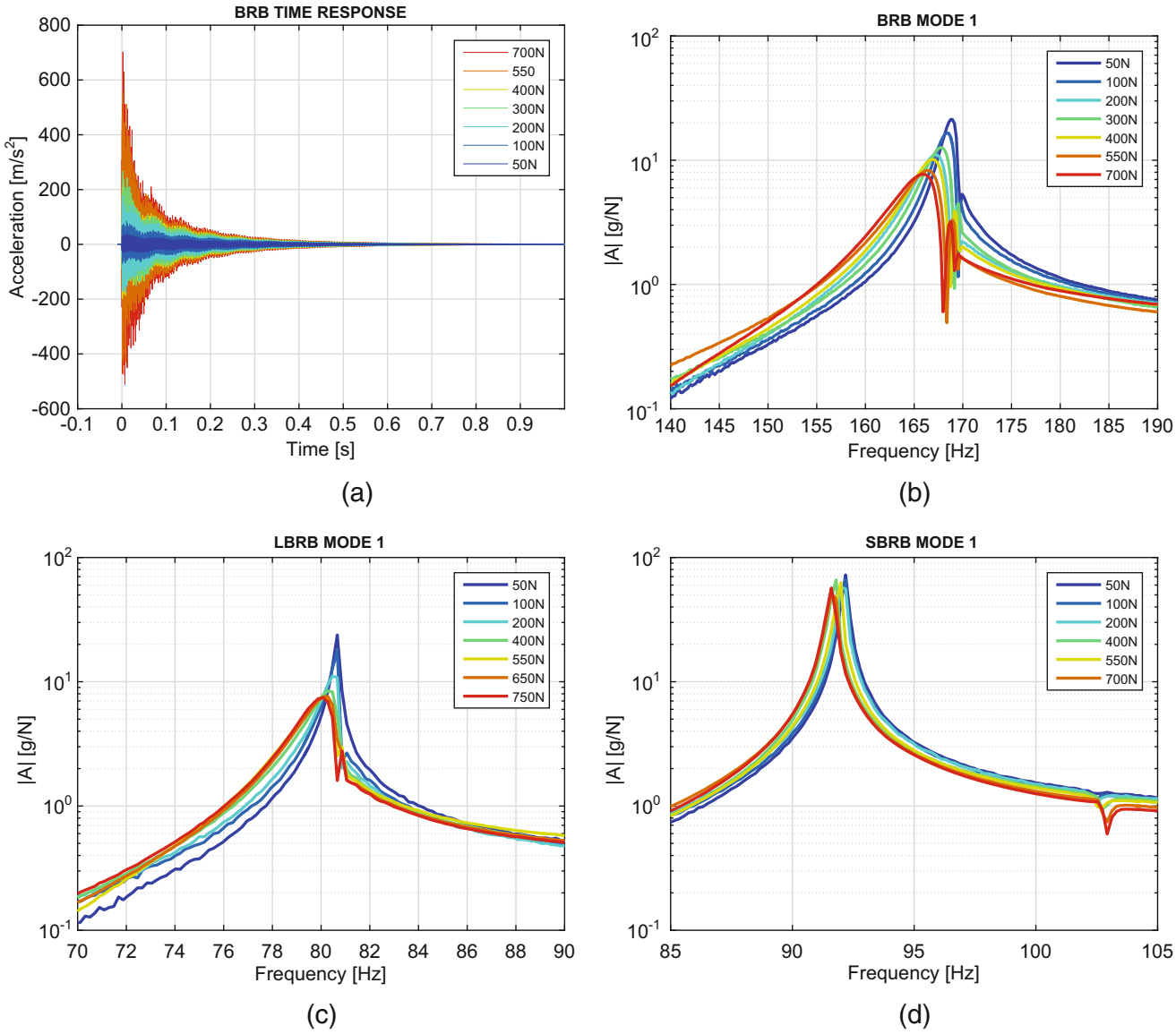

Fig. 7.5 (**a**) Time responses of the BRB at node 8 at different impact forces, and Mode 1 FRFs for (**b**) the BRB, (**c**) the LBRB, and (**d**) the SBRB

frequency range and the impact excitation levels, with the natural frequency decreasing as the impact force increases. For the first mode, for the BRB, LBRB and SBRB, frequency shifts, as estimated by the lcoation of the peak in the FRFs, between the lowest and highest impact force are respectively -2, -1.6 and -0.15%. Thus the BRB has the most nonlinear softening behaviour compared to the other beams.

7.2.3.2 Damping Shift Comparison

Since the amount of energy dissipated in the lap joint configuration depends on the amount of load it carries, it is important to measure and quantify the change in the damping and stiffness properties of the beam caused by the increase in load. In this section of the paper, the percentage shifts in natural frequency and damping ratio are used to quantify the changes in the properties of each beam. The frequency and damping shift are in a percentage form and they are obtained as,

$$f_s = \frac{|f_{min} - f_n|}{f_n} \cdot 100 \quad [\%], \qquad \zeta_s = \frac{|\zeta_{max} - \zeta_L|}{\zeta_L} \cdot 100 \quad [\%]. \tag{7.1}$$

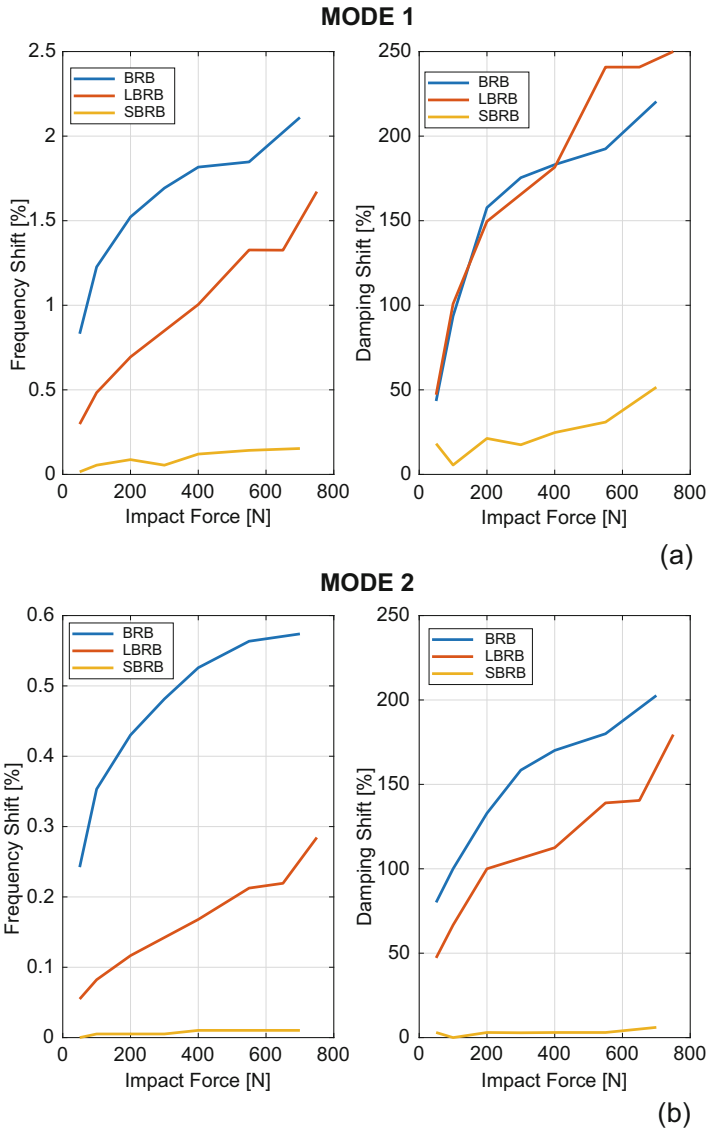

Fig. 7.6 Frequency and damping shift against impact force for Mode 1 (**a**) and Mode 2 (**b**)

The percentage frequency and damping shifts were calculated for the first three modes of each beam as the impact force changes: Fig. 7.6a, b present the frequency and damping percentage shift for all three beams against the impact force level for the first two bending modes. It can be noticed that, for the first mode, BRB shows a high shift in frequency compared to the other beams, while the LBRB shows a larger shift in the damping. Similarly, for the second mode, the shift in frequency and damping is larger for the BRB and LBRB. Turning to the SBRB, this has a very low shift in frequency and damping for the first mode and practically no shift for the second mode, as demonstrated by the constant straight line in Fig. 7.6b. From these observations it's possible to say that the BRB and LBRB structures experience the highest level of nonlinearity as a result of the increase in impact load, while the SBRB shows little or no nonlinear behavior for both modes.

In Fig. 7.7a, b, the frequency and damping shifts for the first three modes are compared against each other for the BRB and LBRB. It can be noticed that, for both beams, the frequency shift experienced by the first mode is significantly higher than the other two modes. The frequency shift for the first mode of the BRB lies between 0.8 and 2.1% while the frequency shifts for the second and third modes fall within 0.2 and 0.5%, hence the shift observed in the first mode is a factor of 4 higher than the shift observed in the other modes. A similar behavior was also observed in the LBRB configuration where the frequency shift for the first mode lies within 0.38 and 1.63%, while the shift experienced by the other modes are within 0.1 and 0.35%. Again, the first mode has a frequency shift of a factor of 4 higher than the other modes. One of the reasons for very high frequency shift observed for the first mode of both beams might be the method used to excite the beams during

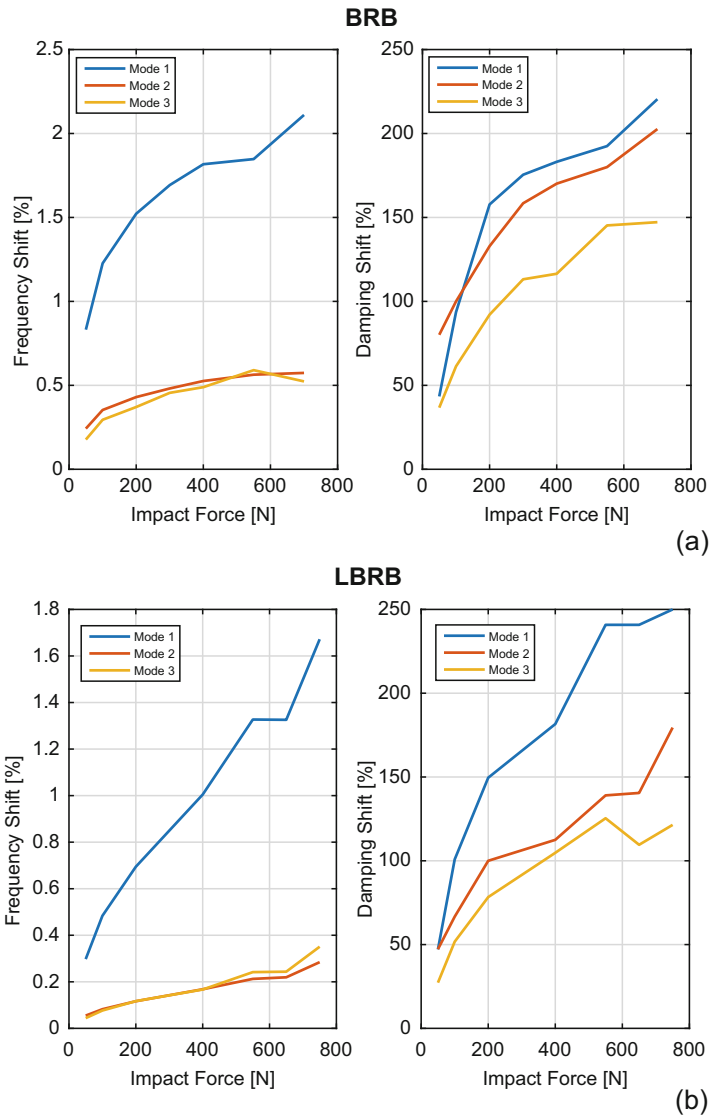

Fig. 7.7 Frequency and damping shift against impact force for BRB (**a**) and LBRB (**b**)

the test, since the energy transferred by the impact hammer to the test structure is not always constant and it can quickly fade out without activating each mode of the structure equally. Hence the higher frequency shift observed on the first mode of each beam can be associated to this effect. However, a different behavior is observed in the damping shift for both beam configurations: in Fig. 7.7a the percentage damping shift for the first two modes are approximately within the same range, while it is slightly lower for mode three. In Fig. 7.7b, for the LBRB, it's possible to see the same behavior, only this time the damping shift is higher for the first mode, while it lies almost on the same range for the other modes. The increase in damping shift with the increase in impact force confirms the high level of nonlinear damping in both beams. The results show the typical behavior found in jointed structures, where the damping nonlinearity can be very high concurrently with a limited frequency nonlinearity.

7.2.4 Nonlinear Characterization Using Hilbert Transform

In order to develop a nonlinear characterization for each beam assembly, a three-step procedure was carried out to identify the frequency and damping behavior at several excitation levels. The first step was a homogeneity check on the FRFs at different excitation levels to detect potential nonlinearities. The second step was a transformation of measured physical

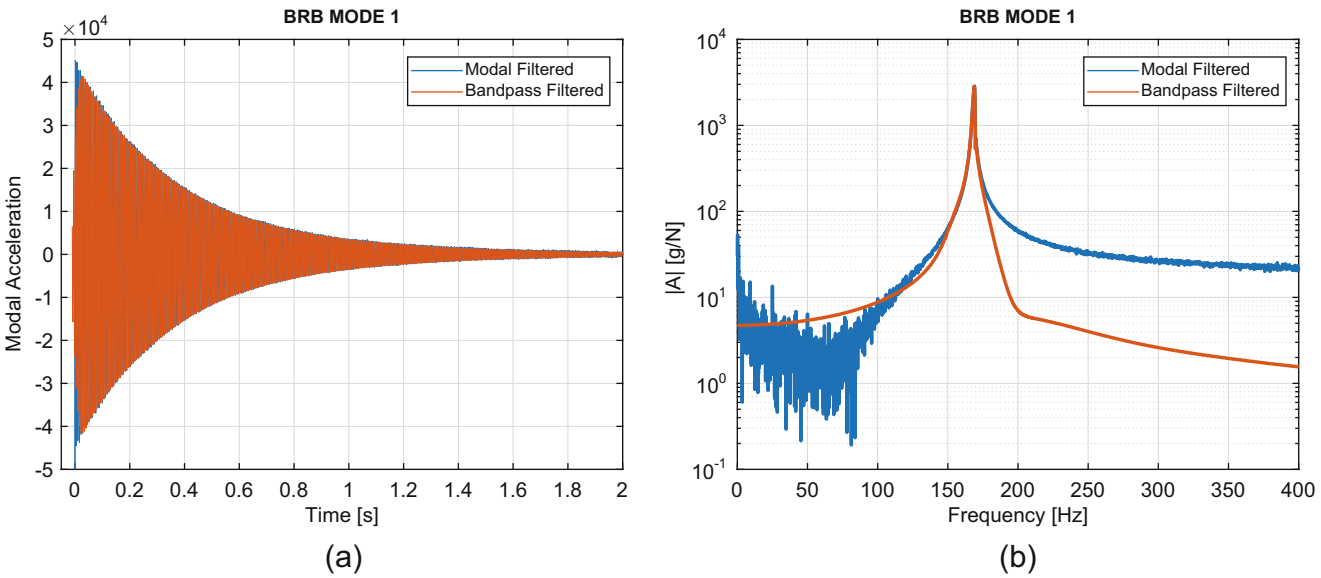

Fig. 7.8 BRB modal filtered and bandpass filtered signal comparison in (**a**) time and (**b**) frequency

data into modal coordinates, performed by applying first a modal filter and then a bandpass one, in order to isolate the contribution of a single mode. The third step consisted of the nonlinear identification and characterization of nonlinearities using the Hilbert Transform (HT). The HT method was used to deduce frequency and damping ratio trends against modal displacement amplitude (see [3–8]).

7.2.4.1 Data Filtering

Prior to the nonlinear characterization of the beams, each measured data was modally filtered, i.e. the data were transformed from physical coordinates into modal coordinates. The modal filter was performed using the physical time series data and the mode shapes matrix obtained previously from the linear modal analysis. After the application of the modal filter, a bandpass filter with an order specified between 4 and 8 was performed on each selected mode of each beam, in order to isolate a single mode in the response. An example of a transformed response after the modal and bandpass filters for the first mode of the BRB is presented in Fig. 7.8, respectively in the time (Fig. 7.8a) and frequency (Fig. 7.8b), domains. Modally filtered data was used for the BRB characterization; however, for the LBRB and the SBRB, the bandpass filter performed better, hence it was used in the characterization section.

7.2.4.2 Nonlinear Characterization

The next step in the experimental investigation was to quantify the change in natural frequency and damping with amplitude. First the Hilbert Transform was applied to the previously obtained modal acceleration data for several modes of each beam system. Then, a 4th order spline fit was applied to the Hilbert amplitude and phase over a selected time window, in order to get the instantaneous damping and frequency, respectively (see [3, 8]). The spline fit serves as a smoothing mechanism in order to estimate the instantaneous damping and frequency; however, because the Hilbert Transform is susceptible to noise at the extremes of the fit, the time window must be carefully selected. Figure 7.9 shows how well the blue filtered modal acceleration is reproduced by the green reconstructed time signal from the fitted Hilbert Transform for the first bending mode of the BRB. The modal velocity and displacement amplitudes V_{fit} and X_{fit} were calculated as,

$$V_{fit} = \frac{A_{fit}}{\omega_{d,fit}}, \qquad X_{fit} = \frac{A_{fit}}{\omega_{d,fit}^2}, \tag{7.2}$$

where A_{fit} and $\omega_{d,fit}$ are the modal acceleration amplitude fit and the instantaneous damped natural frequency obtained from the Hilbert Transform spline fit, respectively.

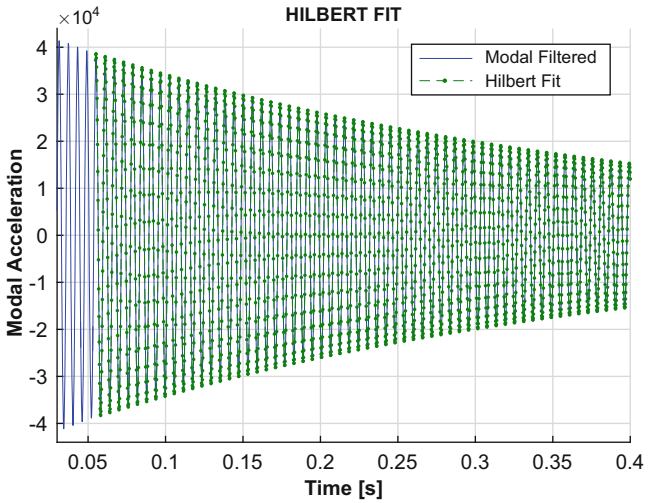

Fig. 7.9 Bandpass filtered modal acceleration and Hilbert fit – BRB Mode 1

Figure 7.10 shows the instantaneous frequency and damping curves against modal displacement amplitude X_{fit} for the first bending mode of the three beams. All three beams show the same softening behavior, with higher impact forces generating higher frequency shifts. The damping behavior exhibited by all three beams shows a power-law relationship, which is dependent on the excitation amplitude. The same analysis was repeated for the second and third modes, for which the damping curves showed the same increasing trend. For mode 3, the Hilbert transform only produced useful results over a range of small amplitudes; however a similar power-law relationship was observed. It is important to point out the fact that the impact point DP is very close to a node of the third mode, especially for the SBRB. As a result of this, the third mode may not have been properly excited and results for this specific mode may be inaccurate.

Comparing the results from the three beams, it is possible to say that the BRB and LBRB graphs show smooth curves and consistent trends at several impact forces, while for the SBRB, the curves are noisier and scattered. This can be due to the fact that, compared to the BRB and LBRB, SBRB shows smaller frequency and damping shifts and to the previously cited Hilbert Transform flaws. A summary of the observed nonlinearities for the three structures is given in Table 7.3; f_n and ζ_L are, respectively, the linear natural frequency and linear damping ratio measured from the flat parts of the frequency-amplitude and damping-amplitude plots, while $f_{n,min}$ and ζ_{max} are the minimum frequency and maximum damping ratio measured from the same plots at the highest impact force.

Further, comparing the damping curves for all three beams directly leads to some interesting conclusions regarding the effect of the far-field structure on the response. Figure 7.11 plots the damping curves for each of the three beams at all forcing levels for the first two bending modes, i.e. all of the nonlinear damping characterizations for the BRB are shown in blue, LBRB in red, SBRB in green. The key observation from these figures is that the three beams, each with a different far-field structure, have very different modal responses. In particular, while the BRB and LBRB exhibit the typical power-law nonlinearity that is consistent with literature, the SBRB shows a roughly linear response. While directly comparing the modal responses for these beams is useful and illuminating, one must keep in mind that the mode shapes for each of these beams are markedly different, as illustrated in Fig. 7.4. At first, this may seem to be an unfair comparison; however, the dependence of the modal response on the mode shape is explored later in the numerical section of this paper in order to draw meaningful conclusions regarding the root-cause of the experimental observations show here.

7.3 Numerical Investigation

From the experimental findings of this work, it is clear that different far-field structures elicit vastly different modal responses; however, this observation alone does not directly confirm or deny the hypothesis that altering the far-field structure changes the way in which the joint is excited or activated. In order to firmly and rigorously arrive at a scientific conclusion, one must "close the loop" by returning to the physical domain and identify a root cause for the experimental observation. The numerical study for this project does just that through validation of the experimental findings.

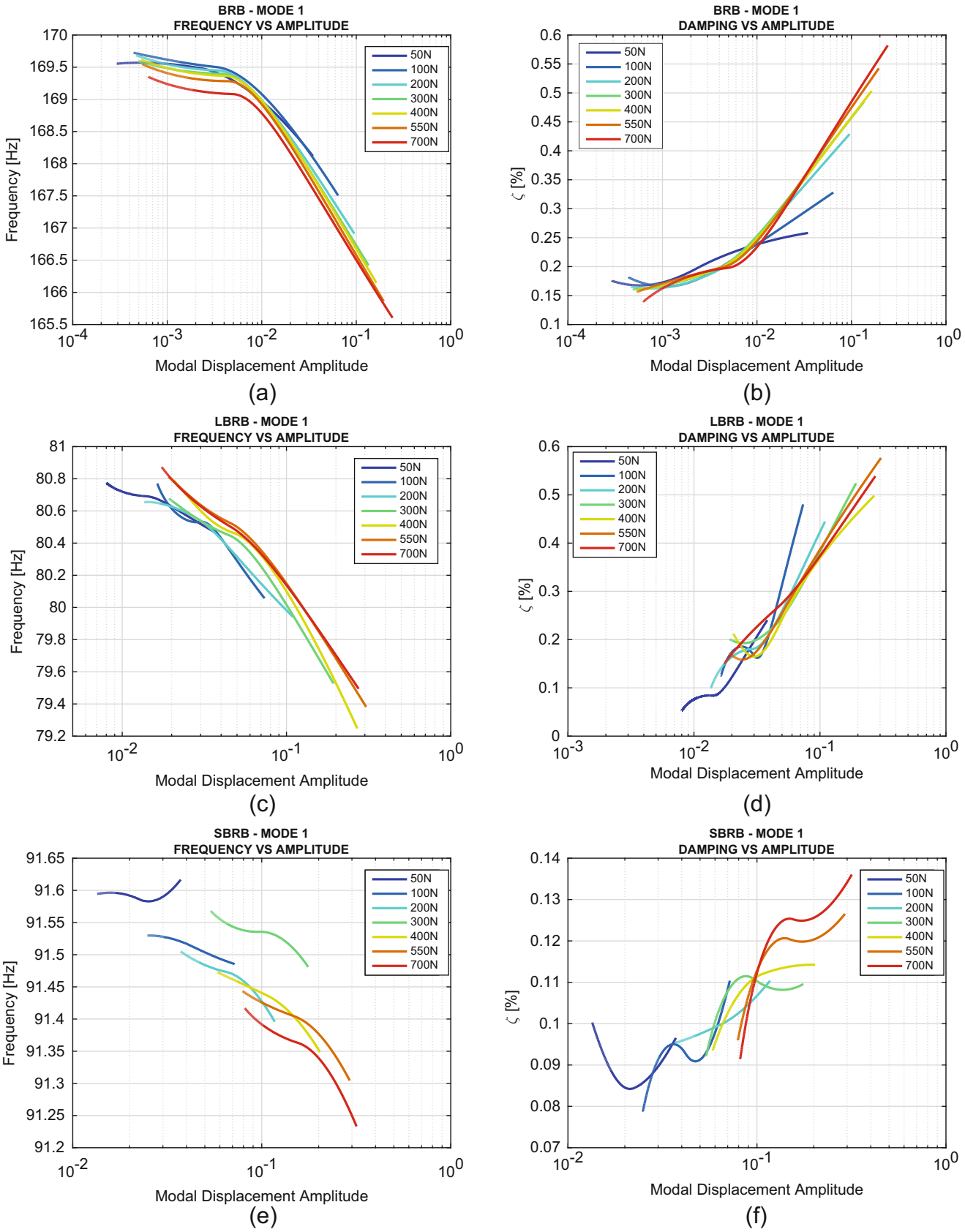

Fig. 7.10 Frequency and damping against modal displacement amplitude for BRB (**a**–**b**), LBRB (**c**–**d**), and SBRB (**e**–**f**)

Table 7.3 Measures of nonlinearities

	MODE	f_n[Hz]	$f_{n,min}$ [Hz]	ζ_L (%)	ζ_{max} (%)
BRB	1	169, 4	165, 6	0, 17	0, 58
	2	585, 7	582, 05	0, 08	0, 23
	3	1185, 5	1178, 2	0, 08	0, 22
LBRB	1	80, 7	79, 4	0, 12	0, 46
	2	291, 7	290, 9	0, 04	0, 11
	3	521, 5	519, 8	0, 06	0, 16
SBRB	1	91, 5	91, 3	0, 10	0, 15
	2	194, 3	194, 3	0, 03	0, 04
	3	496, 1	494, 7	0, 20	0, 44

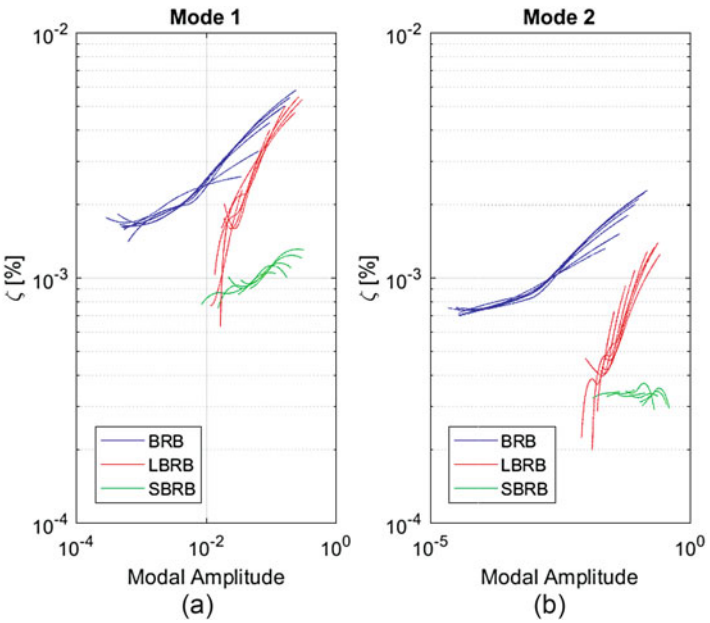

Fig. 7.11 Comparison of the damping ratios as functions of response amplitude for all three beams across all force levels tested for both (**a**) Mode 1 and (**b**) Mode 2

7.3.1 Nonlinear Amplitude Dependent Properties from Quasi-static Finite Element

In this numerical study, discrete, physical four-parameter Iwan elements were implemented into finite element models. It was found that a single set of physical Iwan model parameters can be implemented into two of the different beam structures to match experimental, modal findings. This result lends credibility to the underlying assumption that the joints in the structures are nominally similar, as they can be physically represented by the same set of modeling parameters.

7.3.1.1 Modeling Procedure

To begin, solid finite element model was created in a finite element program, and this model was extracted as a Craig-Bampton reduced-order model into MATLAB. In the finite element program, the two beams were modeled separately and connected with weak springs; Fig. 7.12 shows and example of the mesh used for the beams. Then, in MATLAB, stiffness elements were added between the spidered-joints between the beams; four-parameter Iwan elements were also added along the length of the beam to the five spider patches. Figure 7.13 illustrates the symmetric arrangement of these spider elements.

The parameters of these elements were fine-tuned to match the amplitude dependent information using standard Brake-Reuss beam information provided by the experimental results for the first two modes. The parameters for the four-parameter Iwan models are given in Table 7.4. To do this, rather than computing the dynamic response of the FEM to an impulsive load, a quasi-static loading was applied in the shape of the structure to the FEM model. The loadings were applied at various

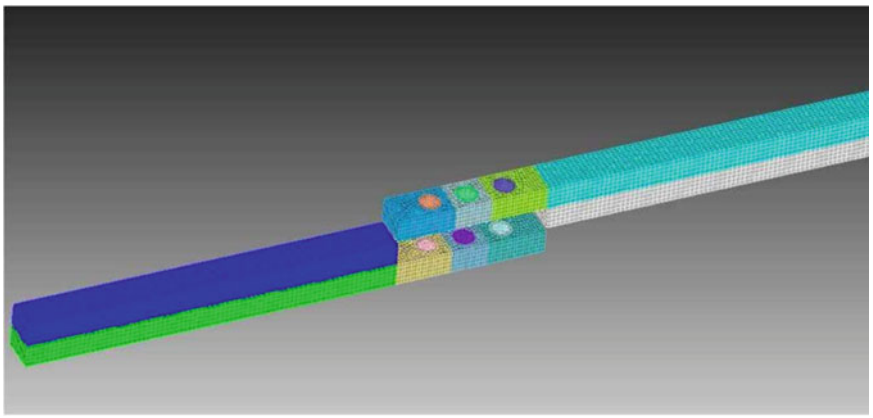

Fig. 7.12 Finite element model with discrete, physical Iwan elements

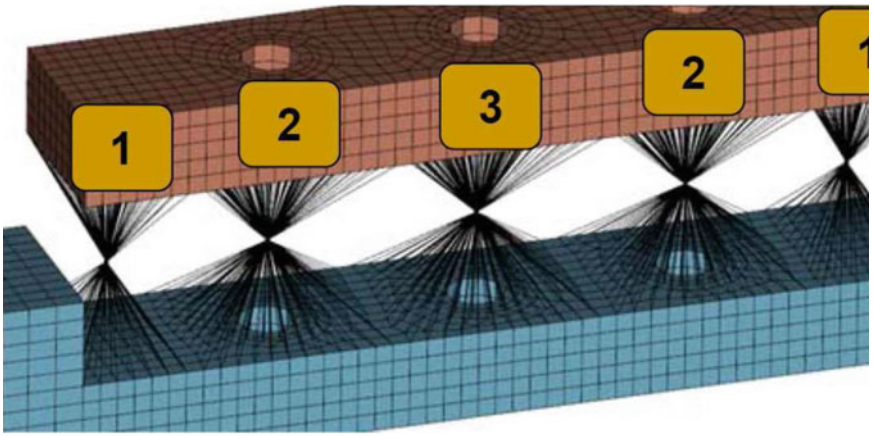

Fig. 7.13 Distribution of spider elements

Table 7.4 Tuned Iwan parameters for quasi-static FEM

Joint ID	F_s	K_t	χ	β
1	35,000	1.5e5	−0.60	0.25
2	35,000	2.2e5	−0.90	0.35
3	1750	2.2e5	−0.15	0.05

amplitudes in order to generate the expected amplitude-dependent curves. Next, the same tuned physical parameters were applied to a model of the LBRB. Using the same quasi-static loading technique based on its mode shapes, modal data for the LBRB model was also recovered.

7.3.1.2 Comparison of Numerical and Experimental Results

Comparisons between the experimental and tuned numerical modal results for the BRB are given in Fig. 7.14. The tuned physical parameters are remarkably effective at capturing the modal responses for the first two modes. Then, using those same identified physical parameters, the comparison of the experimental and numerical results for the LBRB is presented in Fig. 7.15. Without any retuning, the numerical model is still able to recover the experimentally-derived modal results. This result heavily suggests that the joints for these systems are nominally identical, and that it is indeed the far-field structure that is responsible for changing the modal responses for these systems. This work thus serves to validate the experimental findings. Put another way, these data show that the joint model's parameters were not significantly influenced by the far-field structure; however, because the total dynamics of the system are, figuratively, the sum of the joint, that evidently behaves the

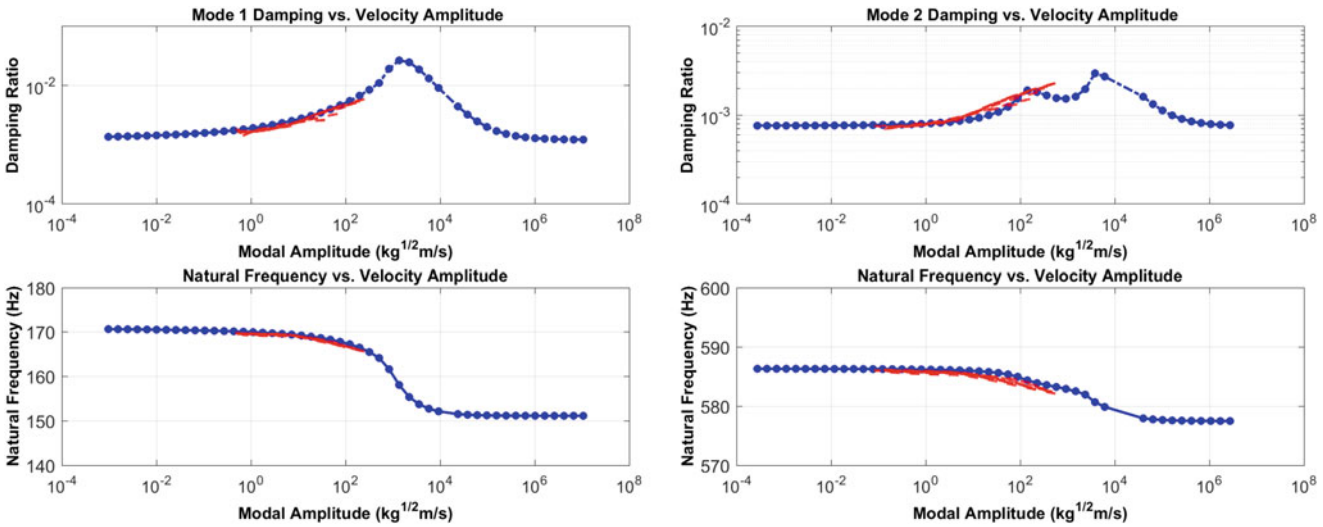

Fig. 7.14 Comparison of numerical and experimental frequency damping curves for the BRB

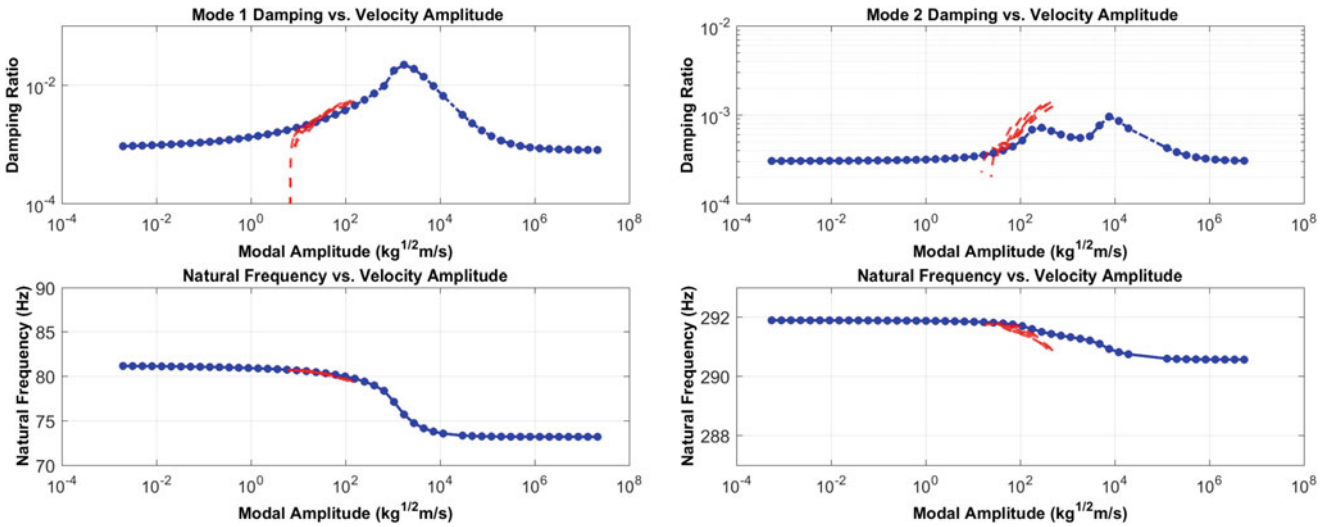

Fig. 7.15 Comparison of numerical and experimental frequency damping curves for the LBRB

same regardless of the far-field structure, and the linear dynamics of the surrounding structure, the modal responses observed experimentally exhibit different characteristics.

7.4 Conclusions

While this work comprises a multitude of techniques, approaches and ideas, it ultimately reduces to a single result. First, it was experimentally observed that the far-field structures of the considered Brake-Reuß beams had significant effects on the modal nonlinear stiffness and damping characteristics of each beam. Then, it was numerically shown that identical physical joint properties can be implemented into the different beam structures to match these experimental modal results without retuning, illustrating that the physical joint properties of these systems are nominally identical. Naturally then, one way to think of each of these systems is the sum of two parts, the nonlinear dynamics of the joint and the linear dynamics of the far-field structure. The ramifications of these results are that physical models of joints can be accurately constructed; however, the parameters must be deduced in the context of the surrounding structure. Thus, to characterize a joint, the *Surrogate System Hypothesis* is proposed:

The Surrogate System Hypothesis states that a surrogate structure, which is easy to model and machine, that contains the same joint as the system of interest can be used to deduce the properties of the joint. These properties, once accounting for the properties of the surrogate structure, can then be substituted directly into the system of interest as a spatially discrete joint model (as opposed to a modal model).

From the modal perspective, relocating the same joint to a new system necessitates the development of a new set of modal joint parameters. In this work, the quasi-static approach in [1] was used to do this. As is done in linear modal substructuring or structural modification, one must recognize that changes to any part of the structure will change the effective modal parameters, and for the nonlinear system, this results in a change to the damping versus amplitude and frequency versus amplitude curves.

Acknowledgements This research was conducted as part of the Nonlinear Mechanics and Dynamics (NOMAD) Research Institute sponsored by Sandia National Laboratories in 2016. Sandia National Laboratories is a multi-mission laboratory managed and operated by Sandia Corporation, a wholly owned subsidiary of Lockheed Martin Corporation, for the U.S. Department of Energy's National Nuclear Security Administration under contract DE-AC04-94AL85000.

Reference

1. Allen, M.S., Lacayo, R.M., Brake, M.R.: Quasi-static modal analysis based on implicit condensation for structures with nonlinear joints. In: The 2016 Leuven Conference on Noise and Vibration Engineering (2016)
2. Breake, M.R., Reuss, P., Segalman, D.J., Gaul, L.: Variability and repeatability of jointed structures with frictional interfaces. In: Allen, M., Mayes, R.L., Rixen, D.J. (eds.) Dynamics of Coupled Structures: Proceedings of the 32nd IMAC, a Conference 2014, Orlando, vol. 1, pp. 245–252. Springer (2014)
3. Deaner, B.J., Allen, M.S., Starr, M.J., Segalman, D.J., Sumali, H.: Application of viscous and Iwan modal damping models to experimental measurements from bolted structures. ASME J. Vib. Acoust. **137**, 021012 (2015)
4. Do, N., Ferri, A.A.: Energy transfer and dissipation in a three-degree-of-freedom system with stribeck friction. In: Proceedings of IMECE 2005, Orlando (2005)
5. Kerschen, G., Worden, K., Vakakis, A.F., Golinval, J.: Past, present and future of nonlinear system identification in structural dynamics. Mech. Syst. Signal Process. **20**(3), 505–592 (2005)
6. Peeters, B., Van der Auweraer, H., Guillaume, P., Leuridan, J.: The polymax frequency-domain method: a new standard for modal parameter estimation? Shock. Vib. **11**, 395–410 (2004)
7. Quinn, D.D.: Modal analysis of jointed structures. J. Sound Vib. **331**(1), 81–93 (2012)
8. Roettgen, D.R., Allen, M.S.: Nonlinear characterization of a bolted, industrial structure using a modal framework. Mech. Syst. Signal Process. **84**(Part B), 152–170 (2017)
9. Segalman, D.J.: A four-parameter Iwan model for lap-type joints. J. Appl. Mech. 72, 752–760 (2005)